https://doi.org/10.5194/egusphere-2026-4232
Preprint. Discussion started: 4 August 2026
© Author(s) 2026. CC BY 4.0 License.

Short-term variations in air-water gas transfer velocity and CO_2 fluxes over a temperate seagrass meadow

Kayleigh E. Granville[1] and Peter Berg[1]

[1]Department of Environmental Sciences, University of Virginia, Charlottesville, 22903, USA

Correspondence to: Kayleigh E. Granville (Kayleigh.Granville@gmail.com)

Abstract. Seagrass meadows store and sequester carbon for long periods of time in their tissues and sediments. They can also emit or take up gases such as carbon dioxide (CO_2) across the air-water interface. Air-water gas fluxes over seagrass meadows are poorly constrained, primarily due to methodological limitations and a persistent lack of fine-scale *in situ* spatial and temporal data. In this study, we present a thorough assessment of air-water CO_2 flux dynamics over a shallow, temperate coastal bay (South Bay, Virginia, USA) that has a benthic environment dominated by a temperate eelgrass meadow (*Zostera marina).* We evaluated major sources of variability in the flux calculation by analyzing *in situ* and regional wind speeds, comparing *in situ* and modeled gas transfer velocities (k_{600}), and conducting a long-term flux study to disentangle diurnal CO_2 flux patterns over South Bay. All wind stations located in proximity to land features significantly underestimated wind speeds over South Bay, while a wind station located in a nearby estuary over open water (Chesapeake Bay) was most representative of *in situ* wind speed measurements. We also derived *in situ* k_{600} by deploying an "upside-down" aquatic eddy covariance system right below the air-water interface and using the data to ground truth the best-fitting empirical parameterizations for our site. The best-fitting models for South Bay were originally derived over the ocean and had an intercept of zero. Using the best-fitting model and continuous water column pCO_2 measurements, we derived hourly air-water CO_2 fluxes over South Bay during the peak seagrass density period (early July) over three years. CO_2 fluxes exhibited a distinct diurnal pattern that correlated well with photosynthetically active radiation, demonstrating that fluxes are driven by photosynthesis and respiration from photosynthetic organisms, seagrasses, epiphytes, benthic microalgae and water column microalgae. Overall, South Bay was a small sink of CO_2 (-0.60 mmol CO_2 m^{-2} d^{-1}) during the peak seagrass period across all three years. Due to the continuous nature of our study, we were able to derive CO_2 flux estimates during a storm period. South Bay was a source of CO_2 during the storm. When the storm period was removed and only fair-weather data were considered, South Bay was a larger sink of CO_2 (-4.20 mmol CO_2 m^{-2} d^{-1}). Our results underline the importance of evaluating air-water gas fluxes over multiple day-night cycles and during multiple weather conditions.

https://doi.org/10.5194/egusphere-2026-4232
Preprint. Discussion started: 4 August 2026
© Author(s) 2026. CC BY 4.0 License.

1 Introduction

Coastal vegetated ecosystems such as seagrass meadows contribute to the global carbon cycle by transporting terrestrial carbon to the ocean and by storing and sequestering organic carbon (C_{org}) (Bianchi et al., 2018; Fennel et al., 2019; Macreadie et al., 2021). The global carbon sequestration capacity of seagrass meadows is uncertain, with global seagrass extent estimates ranging from 16-165 million ha and C_{org} stock estimates ranging from 1,700 to 21,000 Tg C (Macreadie et al., 2021; Prentice et al., 2020). Local- and regional-scale C_{org} stock variability is partially attributed to uncertainties in the air-water carbon dioxide (CO_2), methane (CH_4), and nitrous oxide (N_2O) fluxes over seagrass meadows, which either contribute to or partially offset the carbon sequestration potential of the ecosystem, depending on the direction of the flux (Ricart et al., 2020; Kim et al., 2022; Oreska et al., 2020).

Air-water gas flux estimates are highly variable over seagrass meadows because common methodologies often do not capture the rapid internal cycling of flux drivers such as wind speed, gas concentrations, and temperatures that have previously been documented in seagrass meadows (Berg et al., 2019; Yang et al., 2019; Van Dam et al., 2021; Rosentreter et al., 2021). Additionally, variations in ecosystem metabolism can occur due to changes in photosynthetically active radiation (PAR) and oxygen (O_2) availability, and these changes can significantly influence CO_2 fluxes on hourly, daily, and seasonal scales (Oreska et al., 2020; Ho et al., 2018; Berger et al., 2020). CO_2 uptake can also be partially offset by CO_2 emissions from inorganic carbon burial (C_{inorg}) that are facilitated by calcification and carbonate dissolution, especially in meadows that have active bivalve communities or that are located near coral reefs (Prentice et al., 2020; Saderne et al., 2019).

Variability in air-water gas flux estimates over estuaries is also partially attributed to uncertainties in existing flux methodologies. Common techniques used to directly measure the *in situ* air-water gas flux, including cavity ring-down spectrometry (Ollivier et al., 2022) and floating chambers (Rosentreter et al., 2017; Jeffrey et al., 2018), usually only provide several hours of flux estimates on fair-weather days. These measurements are often not representative of fluxes over full tidal, diurnal, and annual cycles, or during poor-weather periods. Eddy covariance towers deployed over estuaries measure fluxes at fine temporal scales for longer periods of time but have high start-up and maintenance costs (Van Dam et al., 2021). Upside-down aquatic eddy covariance (UAEC) systems can measure fluxes across the air-water interface as well, but this technique has not yet been applied in a tidal estuary for CO_2 flux measurements (Berg et al., 2017, 2020; Long and Nicholson, 2018).

As a result, air-water gas exchange over longer time periods is frequently estimated by a simple mass transfer equation such as Eq. (1):

$$F = k * (C_w - C_0), \quad (1)$$

where F is the air-water gas flux (mass area^{-1} time^{-1}), k is the gas transfer velocity (length time^{-1}), C_w is the bulk concentration of the gas in the water column (mass volume^{-1}), and C_0 is the air-equilibrium concentration of the gas at the air-water interface (mass volume^{-1}) (Cole et al., 2010; Garcia and Gordon, 1992; Wanninkhof, 2014). The gas transfer velocity is regarded as the primary source of uncertainty in this calculation because it describes the complex movement of the gas through the boundary layers on either side of the air-water interface. Due to the much lower gas diffusivity of sparingly dissolved gasses such as

CO_2 on the water side, the dominant resistance to gas transport is found in this boundary layer (Wanninkhof et al., 2009). This process can be influenced by multiple environmental variables and is therefore difficult to measure (Wanninkhof, 1992; Vieira Borges et al., 2004; Ho et al., 2006; Wanninkhof et al., 2009). Thus, k is typically parameterized as a function of one or multiple environmental variables. These empirical parameterizations are usually presented as k_{600} or k_{660} models, where 600 and 660 are the Schmidt numbers for CO_2 at 20°C in freshwater and seawater, respectively (Wanninkhof, 2014; Ho et al., 2011).

Selecting a k_{600} or k_{660} model that is representative of environmental conditions in a seagrass meadow involves several considerations. Many empirical relationships commonly used for fetch-limited systems are derived from parameterizations of wind speed scaled to 10 m above the ground (U_{10}) (Frankignoulle and Borges, 2001; Borges et al., 2018; Ollivier et al., 2022). A number of these well-tested wind-based empirical relationships were derived over the open ocean, where wind is the major driver of gas exchange for slightly soluble gases (Wanninkhof et al., 2009; McGillis et al., 2004; Ho et al., 2006; Nightingale et al., 2000). However, wind-based empirical relationships derived over the open ocean lack observational data when $U_{10} < 4$ m s^{-1}, a value that estuarine wind speeds are often at or below (Wanninkhof et al., 2009; Dobashi and Ho, 2023; Ho et al., 2018). Further, evidence suggests that other variables such as current velocity and water depth may be major drivers of gas transfer velocity in shallow fetch-limited environments such as mangrove estuaries and seagrass meadows (Rosentreter et al. 2017; Ho et al., 2016). Water depth and current velocity can be more difficult to constrain than wind speed estimates, which are generally available from regional wind stations or global models (Wanninkhof, 2014; Rosentreter et al., 2017; Ho et al., 2016). Whether these regional or global data are representative of *in situ* conditions is also a consideration. There is an implicit assumption that the most appropriate wind data over estuaries are those collected closest to the study area, but this assumption does not consider the potential reductions in wind speed over land due to increased bed stress (Lawson et al., 2007; Mariotti et al., 2018).

Here, we thoroughly assess air-water CO_2 flux dynamics over a shallow, temperate seagrass meadow (South Bay, Virginia, USA) by evaluating major sources of variability in the flux calculation and by deriving hourly CO_2 fluxes during the peak seagrass density period over multiple years. Through a comparison of *in situ* and regional wind speed measurements, we determine the ability of regional wind stations on land to predict *in situ* wind speeds in South Bay. Using upside-down aquatic eddy covariance, we derived k_{600} values from *in situ* air-water O_2 flux measurements. We compared *in situ* k_{600} values derived at wind speeds ≤ 4.5 m s^{-1} to modelled k_{600} values, and determined which k_{600} models were representative for our system. Finally, we used the wind speed comparison and k_{600} model analysis to report three years of diurnal CO_2 fluxes during the peak seagrass density period (July) at our site.

https://doi.org/10.5194/egusphere-2026-4232
Preprint. Discussion started: 4 August 2026
© Author(s) 2026. CC BY 4.0 License.

2 Methods

2.1 Study site

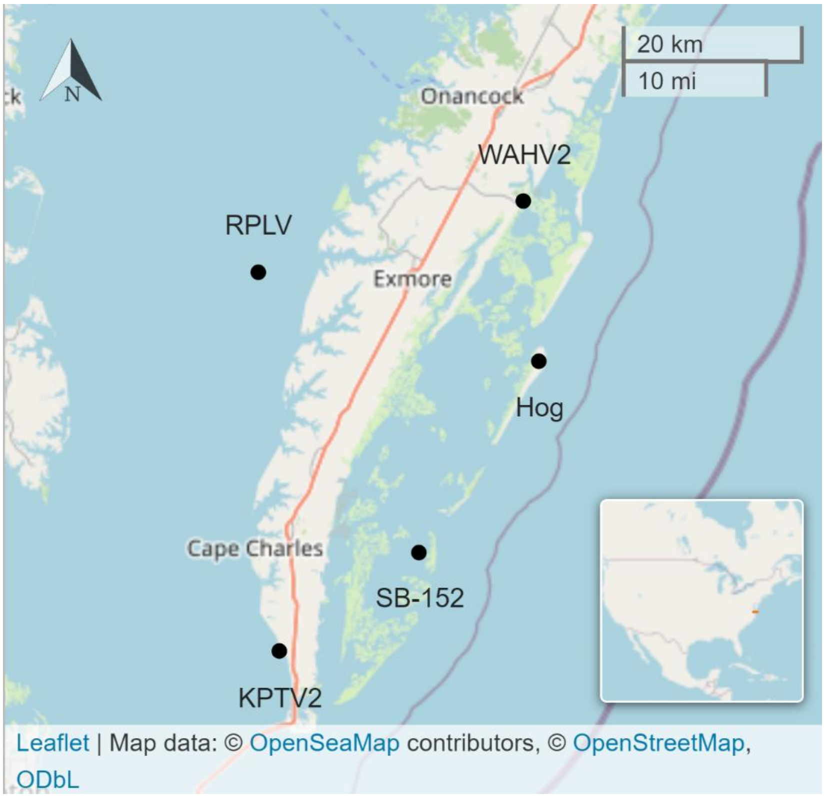

Figure 1: Map of the study site and regional wind stations. The study site (SB-152) is located in central South Bay within the Virginia Coast Reserve (VCR), a series of barrier islands and shallow coastal lagoons located offshore of the Delmarva peninsula. The Wachapreague regional wind station (WAHV2, NOAA NDBC) is located over a channel north of the VCR. The Hog station is located on Hog Island, a barrier island in the VCR (Hog, VCR Long-Term Ecological Research site). Kiptopeke is located at the land-water interface of the Chesapeake Bay (KPTV2, NOAA NDBC KPTV2), to the west of the Delmarva peninsula. Rappahannock Light is located offshore in the Chesapeake Bay (RPLV2, NOAA NDBC RPLV2).

South Bay is a shallow coastal lagoon in the Virginia Coast Reserve (VCR), located offshore of the Delmarva peninsula in the Mid-Atlantic region of the United States (Fig. 1). South Bay has a tidal range of 1.2 m and an average water depth of 1.0 m below mean sea level, is bordered by a barrier island with a back-barrier marsh (Wreck Island) to the east, and is connected to the Atlantic Ocean by two inlets at the north and south (Fig. 1) (Reidenbach and Thomas, 2018). The meadow has minimal anthropogenic influence and no significant freshwater inputs. Wind is the dominant forcing on water circulation and has a strong seasonality, with southerly winds typically occurring in the summer and northerly winds typically occurring in the

https://doi.org/10.5194/egusphere-2026-4232
Preprint. Discussion started: 4 August 2026
© Author(s) 2026. CC BY 4.0 License.

winter (Wiberg et al., 2015; Fagherazzi and Wiberg, 2009). The benthos is dominated by a *Zostera marina* meadow that is the result of a successful seagrass restoration project (McGlathery et al., 2012; Orth et al., 2020). The seagrass meadow exhibits a typical growth pattern for temperate seagrasses and seagrass densities peak around 400 – 550 shoots m^{-2} in early July (Aoki et al., 2021; Rheuban et al., 2014; Berger et al., 2021). The average C_{org} sequestration rate of the meadow was 1070 t CO_2 yr^{-1} from 2013-2016 (Oreska et al., 2020). Significant C_{inorg} burial has not been observed (Saderne et al., 2019; Oreska et al., 2020). Century-scale stored C_{org} originating from *Z. marina* was also identified below the seagrass meadow through dating 2.2 m deep sediment cores (Berg et al., 2025). In some cases, the stored C_{org} was double the amount buried in the sediments of the modern meadow (Berg et al., 2025). Our primary site is in the central area of the seagrass meadow (SB-152, 37.261881 N, 75.815125 W) (Fig. 1), where our *in situ* wind measurements were collected, our UAEC system was deployed to assess *in situ* k values, and our CO_2 fluxes were derived. SB-152 is also the site of over a decade of ecosystem metabolism measurements conducted with the aquatic eddy covariance technique (Hume et al., 2011; Rheuban et al., 2014; Berg et al., 2019, Berger et al., 2020).

Four geographically distinct regional wind stations that are located in or near the VCR and that could be representative of wind speed and direction over South Bay were included in the regional wind analysis (Fig. 1). Three of these stations are owned and maintained by NOAA's National Ocean Service Water Level Observation Network. "Wachapreague" is located over a channel in the VCR (NOAA NDBC Station WAHV2; 37.608 N, 75.686 W). "Kiptopeke" is located at the land-water interface of the Chesapeake Bay (NOAA NDBC Station KPTV2; 37.165 N, 75.988 W). "Rappahannock Light" is an open-water station located in the Chesapeake Bay ("Rappahannock Light", NOAA NDBC RPLV2; 37.538 N, 76.014 W) (Fig. 1). The final station, "Hog" Island, is located over a barrier island in the VCR and is maintained by the VCR Long-Term Ecological Research site (VCR-LTER) (37.45052 N, 75.6668 W).

2.2 Comparison of *in situ* and regional winds

Regional and *in situ* wind speeds were compared for 5-7 days per month in June, July, August, and October of 2022. *In situ* wind speeds and directions over SB-152 were measured at a 1-minute resolution with a compact anemometer (WindLog data logger, RainWise). The compact anemometer was mounted at SB-152 approximately 2.5 m above the sediment surface on a PVC pole. Wind speeds were rescaled to a 10 m height (U_{10}) following Mariotti et al. (2018):

$$U_{10} = \frac{U_z * \log(\frac{10}{z_0})}{\log(\frac{z}{z_0})} , \qquad (2)$$

where z is the height of the wind sensor above the water (m) and z_0 is the roughness coefficient (0.002 m). Changes in z were accounted for with water depth measurements that were taken at 1-minute intervals with a water level data logger (HOBO U20-04, Onset). *In situ* U_{10} measurements were averaged to 1-hour intervals to reduce noise.

Existing regional wind speed and direction measurements were collected from the four geographically distinct regional wind stations. 6-minute resolution measurements were available for the Wachapreague (NOAA NDBC Station WAHV2), Kiptopeke

https://doi.org/10.5194/egusphere-2026-4232
Preprint. Discussion started: 4 August 2026
© Author(s) 2026. CC BY 4.0 License.

(NOAA NDBC Station KPTV2), and Rappahannock Light (NOAA NDBC Station RPLV2) stations (Fig. 1). 1-hour resolution measurements were available for the Hog Island station (VCR-LTER, knb-lter-vcr.25.49) (Fig. 1). All wind speed measurements were rescaled to U_{10} (Eq. 2) and averaged to a 1-hour resolution for comparison with the *in situ* wind speed measurements.

Hourly wind speed and direction estimates were also collected from the ERA5 reanalysis, a global climate and weather reanalysis product that combines model data with observations to provide hourly estimates for a large number of atmospheric, ocean-wave, and land-surface quantities, including wind speed and direction, on a regular latitude-longitude grid of 0.25 degrees (Copernicus Climate Change Service, 2023; Hersbach et al. 2017). These estimates were also compared to the *in situ* and regional wind data to assess the fit of the reanalysis to wind speed and direction over South Bay. Pairwise Wilcoxon rank-sum tests were conducted to compare the regional stations and the ERA5 reanalysis to the *in situ* measurements. All analyses were performed using R statistical software, primarily with the "tidyverse" and "stats" packages (v4.4.2, R Core Team, 2024; Wickham et al., 2019).

2.3 *In situ* gas transfer velocity estimates

To estimate *in situ* k values for CO_2 (k_{CO_2}), we first estimated *in situ* k values for O_2 (k_{O_2}) from high-frequency air-water O_2 fluxes measured using the UAEC technique at SB-152 (Berg et al., 2020; Long and Nicholson, 2018; Berg and Pace, 2017). Briefly, the UAEC technique measures the three-dimensional current velocity field using an acoustic Doppler velocimeter (ADV) equipped with a cabled sensor head positioned upward (Vector, Nortek AS), and water column O_2 concentrations using a fast-responding O_2 sensor that is standard for aquatic eddy covariance located ~10 cm below the air-water interface (Fig. 2) (Berg et al., 2003, 2022; Berg and Pace, 2017). An important consideration for UAEC is that turbulent heat fluxes at the air-water interface, unlike those typically found in the benthic environment, can be substantial (Berg et al., 2020). Fast-responding O_2 sensors are inherently sensitive to temperature changes, so O_2 sensor readings must be corrected with parallel high-speed temperature measurements to prevent temperature bias in the O_2 eddy flux calculation (Berg et al., 2020; Granville et al., 2023). Thus, we used a fast-responding dual O_2-temperature planar optode sensor that measured O_2 and temperature at the same point in the water column for this study (Fig. 2b) (RINKO, JFE Advantech). We also independently measured water column O_2 concentrations and temperatures with slow-responding but stable oxygen optodes at a 1-minute resolution (miniDOT, PME). The UAEC system was mounted to a stainless steel pole with a custom mounting device that allowed the system to slide up and down the pole with tidal height (Fig. 2a). Two buoys and a rudder held the system at a fixed point beneath the water surface, oriented into the main current (Fig. 2a). O_2 fluxes were extracted from the eddy covariance data, quality-controlled, and binned into 15-minute intervals following protocols described in detail in Berg and Pace (2017) and Berg et al. (2022). The UAEC system measured high-quality O_2 fluxes when wind speeds were ≤ 4.5 m s^{-1}. For the purpose of this analysis, we selected a 4-hour deployment period when wind speeds consistently met this condition (26 August 2021, 02:45 – 06:45 AM EDT).

https://doi.org/10.5194/egusphere-2026-4232
Preprint. Discussion started: 4 August 2026
© Author(s) 2026. CC BY 4.0 License.

We then used Eq. 1 to calculate *in situ* k_{O_2} values, where F was the O_2 flux measured by the UAEC system, C_w was the water column O_2 concentration measured with the stable optode, and C_0 was the air-equilibrium concentration of O_2 derived within the UAEC analysis software (Peter Berg, unpublished). The k_{O_2} values were converted to k_{CO_2} following Eq. 3:

$$\frac{k_{O_2}}{k_{CO_2}} = \left(\frac{Sc_{O_2}}{Sc_{CO_2}}\right)^n, \qquad (3)$$

where the value of -0.5 was used for n to be consistent with other low-wind systems, and Sc_{O_2} and Sc_{CO_2} were the Schmidt numbers for O_2 and CO_2, respectively (Cole et al., 2010). Sc_{O_2} and Sc_{CO_2} were derived from *in situ* water temperature measurements collected with the stable optodes, a standard salinity estimate for South Bay (31 ppt), and well-established solubility coefficients for O_2 and CO_2 (Wanninkhof, 2014; Jähne et al., 1987; Garcia and Gordon, 1992; Weiss, 1974).

k_{CO_2} values were also normalized to k_{600} for comparison with the k_{600} models (Cole et al., 2010):

$$k_{600} = k_{CO_2} * \left(\frac{600}{Sc_{CO_2}}\right)^n \qquad (4)$$

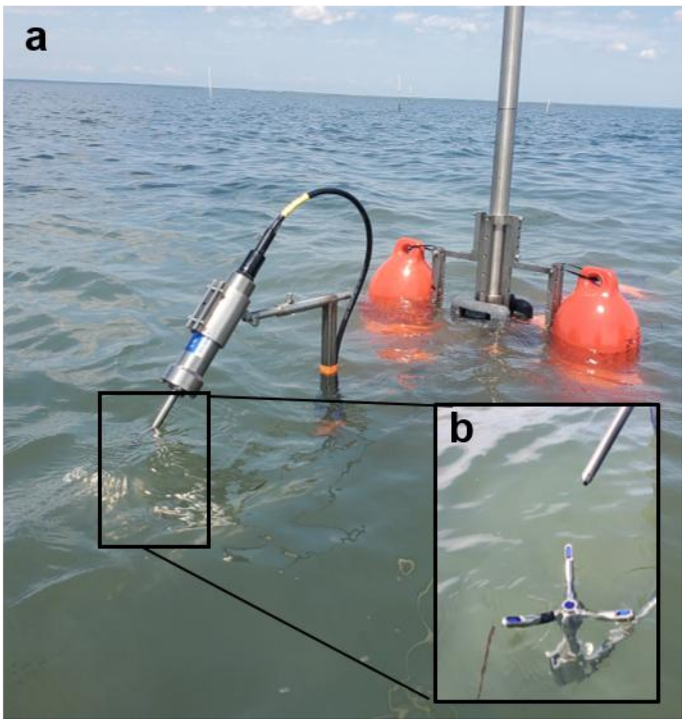

Figure 2: (a) The upside-down aquatic eddy covariance (UAEC) system deployed in South Bay. The system was custom-mounted to a stainless-steel pole and slid up and down with tidal height. Two buoys and a rudder held the system in a fixed location under the water's surface, oriented into the main current. (b) A visual of the acoustic Doppler velocimeter (ADV) equipped with a cabled sensor head positioned upward and a fast-responding O_2 sensor that is standard for aquatic eddy covariance.

https://doi.org/10.5194/egusphere-2026-4232
Preprint. Discussion started: 4 August 2026
© Author(s) 2026. CC BY 4.0 License.

2.4 Comparison of *in situ* and modelled gas transfer velocity

To compare *in situ* k_{600} values with k_{600} values derived from published models, we identified 11 wind-based empirical parameterizations, 1 parameterization derived from water depth and current velocity, and two parameterizations derived from wind speed, water depth, and current velocity that had been designed for seagrass meadows or that had previously been established for use over shallow fetch-limited estuaries comparable to our site (Table 1). All k_{660} models were normalized to k_{600} assuming a Schmidt number of n = -0.5 (Eq. 4). The mean k_{660} and relative root-mean-square-error (rRMSE) were derived during the August 2021 for each parameterization and compared to the *in situ* k_{600} values to determine the best-fitting models for our site (Table 1).

Table 1: For each empirical parameterization, the analysis code, the reference, and the original k_{600} or k_{660} model equation is provided. All equations were standardized to k_{600} for our analysis. U_{10} is wind speed scaled to a height of 10 m above the water surface (m s^{-1}), v is current velocity (cm s^{-1}), and h is water depth (m). The mean k_{600} (m s^{-1}) during the August 2021 upside-down aquatic eddy covariance deployment, as well as the relative root-mean-square-error (rRMSE, %) of the *in situ* and modeled data, is shown for each parameterization. ****Note: B04a was not included in Figure 5a because the overestimation of the*** **in situ** ***k_{600} was out of view on the plot.***

Parameterization		Equation	Mean k_{600}	rRMSE
Wind speed parameterizations				
N00	Nightingale et al. 2000	$k_{600} = 0.333U_{10} + 0.222{U_{10}}^2$	3.13 ± 0.264	0.685
M01	McGillis et al. 2001	$k_{660} = 3.3 + 0.026{U_{10}}^3$	4.15 ± 0.128	1.26
RC01	Raymond and Cole 2001	$k_{600} = 1.58e^{0.3U_{10}}$	3.99 ± 0.188	1.12
M04	McGillis et al. 2004	$k_{660} = 8.2 + 0.014{U_{10}}^3$	8.66 ± 0.0691	4.20
B04	Vieira Borges et al. 2004	$k_{600wind} = 1.0 + 2.58U_{10}$	8.82 ± 0.395	4.28
H06	Ho et al. 2006	$k_{600} = (0.266 \pm 0.019){U_{10}}^2$	2.54 ±0.256	0.598
J08	Jiang et al. 2008	$k_{600} = 0.314{U_{10}}^2 - 0.436U_{10} + 3.990$	5.67 ± 0.235	2.16
W09	Wanninkhof et al. 2009	$k_{660} = 3 + 0.1U_{10} + 0.064{U_{10}}^2 + 0.011{U_{10}}^3$	4.47 ± 0.135	1.44
H11	Ho et al. 2011	$k_{600} = (0.262 \pm 0.022){U_{10}}^2$	2.50 ± 0.252	0.603
W14	Wanninkhof 2014	$k_{660} = 0.251{U_{10}}^2$	2.51 ± 0.253	0.601
D23	Dobashi and Ho 2023	$k_{600} = 0.143{U_{10}}^2$	1.37 ± 0.137	1.12
Multi-variable parameterizations				
B04c	Vieira Borges et al. 2004	$k_{600current} = 1.719v^{0.5}h^{-0.5}$	3.95 ± 0.252	1.05

https://doi.org/10.5194/egusphere-2026-4232
Preprint. Discussion started: 4 August 2026
© Author(s) 2026. CC BY 4.0 License.

*B04a**	Vieira Borges et al. 2004	$k_{600all} = 1.0 + 1.719v^{0.5}h^{-0.5} + 2.58U_{10}$	9.77 ± 0.378	4.95
H16	Ho et al. 2016	$k_{600} = 0.77w^{0.5}h^{-0.5} + 0.266{U_{10}}^2$	4.31 ± 0.332	1.22

2.5 Diurnal CO_2 flux estimates

We derived hourly air-water CO_2 fluxes over SB-152 during the peak seagrass density period across three years. Deployments occurred for 3 days in 2021 (10:00 EDT on 14 July 2021 – 10:00 EDT on 17 July 2021), 5 days in 2022 (08:30 EDT on 6 July 2022 – 12:30 EDT on 11 July 2022), and 6.5 days in 2023 (16:00 EDT on 4 July 2023 – 09:00 EDT on 11 July 2023). The air-water CO_2 flux was calculated every minute following:

$$FCO_2 = K_0 * kCO_2 * (pCO_{2w} - pCO_{2a}), \tag{5}$$

Where FCO_2 is the air-water CO_2 flux (mmol m^{-2} min^{-1}), K_0 is the gas solubility based on temperature and salinity (mmol m^{-3} atm^{-1}), kCO_2 is the gas transfer velocity at the air-water interface (m min^{-1}), and pCO_{2w} and pCO_{2a} are the partial pressures of CO_2 in the water column and overlying air, respectively (atm) (Wanninkhof, 1992; Mu et al., 2014). K_0 was derived from *in situ* temperature and salinity data using a modified form of Henry's law (Weiss, 1974; Wanninkhof, 2014). Temperature was measured at 1-minute intervals with a stable O_2 optode (miniDOT, PME) mounted at mid-canopy height (30 cm above the seafloor). Salinity was also measured at mid-canopy height using a salt water conductivity logger (HOBO U24-002-C, Onset) in 2023 and a pH sensor in 2022 (SeapHOx V2, SeaBird Scientific). Salinity measurements were unavailable in 2021 and for three days in 2022, so a standard value for South Bay was used (31 ppt).

kCO_2 values were derived once per minute using a best fitting k_{600} model determined by our k_{600} model analysis and *in situ* wind speed data collected once per minute over SB-152 with a compact anemometer as described above (WindLog data logger, RainWise). *In situ* wind speed data were not available for 2021, so wind data were collected from Rappahannock Light (NOAA NDBC RPLV2), the best-fitting regional wind station. The k_{600} values were converted to kCO_2 using Sc_{CO_2} numbers derived from our *in situ* temperature and salinity data throughout the deployment (Eq. 4).

pCO_{2w} was derived from continuous measurements (every 2 seconds) of dissolved pCO_{2w} (ppm) that were corrected for temperature and pressure variations with an autonomous, submersible infrared sensor that is well-suited for shallow, high-variability environments (miniCO_2, Pro Oceanus Systems Inc.). The infrared sensor had a measurement range of 0-2000 ppm pCO_2, an accuracy of 2 % of the maximum range, a sample rate of 2 s, and a resolution of 0.1 % of the maximum range. pCO_2 measurements were validated using DIC bottle samples collected at our site. Atmospheric CO_2 mole fractions were retrieved from the NOAA Carbon Tracker Near-Real Time (CT-NRT.v2023-5) and converted to pCO_{2a} using barometric pressure measured over the VCR (knb-lter-vcr.307.5) and water vapor pressure, which was derived from the *in situ* temperature and salinity measurements using the R "seacarb" package (Gattuso et al., 2024; Mu et al., 2014; Weiss and Price, 1980). The 1-minute fluxes were summed to hourly values for analysis.

https://doi.org/10.5194/egusphere-2026-4232
Preprint. Discussion started: 4 August 2026
© Author(s) 2026. CC BY 4.0 License.

We also measured photosynthetically active radiation (PAR) with a LI-192 underwater quantum sensor (miniPAR, PME) and water column O_2 concentrations with a stable O_2 optode (miniDOT, PME) once per minute at mid-canopy height throughout all deployments. During each deployment, we counted seagrass shoot densities by hand. All analyses were performed using R statistical software, primarily with the "tidyverse" package (v4.4.2, R Core Team, 2024; Wickham et al., 2019). All mean values are reported as the mean ± standard deviation.

3 Results

3.1 Comparison of *in situ* and regional winds

When regional and *in situ* wind speeds were compared in 2022, *in situ* wind speeds measured over SB-152 were not significantly different than wind speeds measured at the open water station (Rappahannock Light) or those reported by the ERA5 reanalysis (Table 2). The three stations located near land underestimated the *in situ* wind speeds across all deployments: wind speeds were underestimated by an average of 33% by the land-water interface station (Kiptopeke), 43% by the channel station (Wachapreague) and 68% by the barrier island station (Hog) (Table 2). Time series data of the July 2022 deployment are shown to demonstrate the variability across stations (Fig. 3, Table 2). The empirical relationship between U_{10} and k_{600} is often represented by a quadratic or power function, so using the stations located near land to estimate *in situ* wind speeds over South Bay would significantly under-estimate k_{600} and the flux calculation (Ho et al., 2011). For SB-152, the Rappahannock station and the ERA5 reanalysis produced the best-fitting wind speed measurements compared to the other regional stations.

Table 2: The number of observations (n), mean, and standard deviation (sd) of hourly wind speeds scaled to a height of 10 m (U_{10}, m s^{-1}) is reported for the *in situ* station, the regional stations, and the ERA5 reanalysis for the 2022 study period (June, July, August, and October 2022). For each regional station and the ERA5 reanalysis, the mean percent difference from the *in situ* wind station (%) is provided, as well as the p value resulting from the pairwise Wilcoxon rank-sum tests with the *in situ* wind station (significance level p > 0.05).

Site	n	Mean	sd	Percent difference	p value
SB-152 (in situ)	485	4.99	2.36	-	-
Rappahannock	485	4.79	2.48	3.8	0.19
Kiptopeke	485	3.34	1.71	33	$3.7 * 10^{-29}$
Wachapreague	485	2.84	2.16	43	$2.3 * 10^{-47}$
Hog	485	1.60	0.88	68	$5.6 * 10^{-116}$
ERA5 Reanalysis	485	4.85	2.42	2.7	0.42

https://doi.org/10.5194/egusphere-2026-4232
Preprint. Discussion started: 4 August 2026
© Author(s) 2026. CC BY 4.0 License.

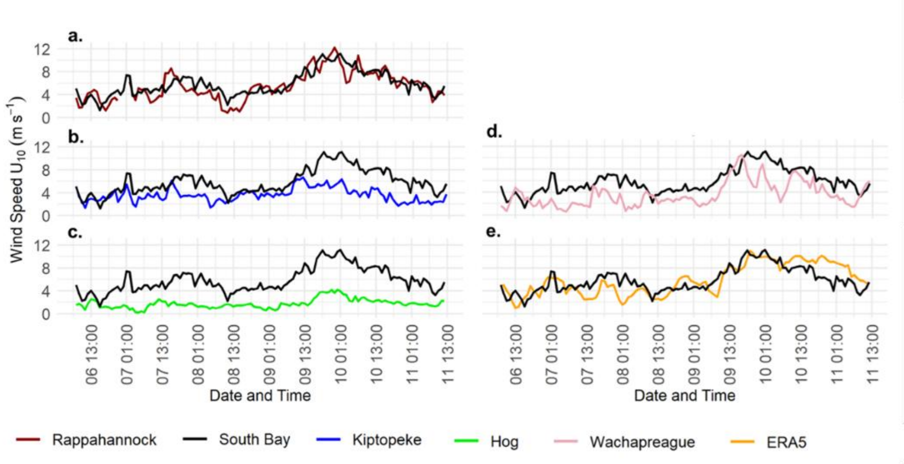

Figure 3: The July 2022 time series of *in situ* wind speeds measured over South Bay was compared to wind speeds reported at the following wind stations: a) Rappahannock, b) Kiptopeke, c) Hog, and d) Wachapreague, as well as e) by the ERA5 reanalysis product. All wind speeds were converted to U_{10}. See Figure 1 for wind station locations.

3.2 *In situ* and modeled gas transfer velocities over SB-152

3.2.2 Variability in modeled gas transfer velocity

From all *in situ* wind speed data collected during the peak seagrass density deployments in 2021, 2022, and 2023, the mean wind speed was U_{10} = 4.95 ± 2.01 m s^{-1}, indicating that wind speeds over South Bay are generally low. We derived k_{600} values for these deployments using eleven well-established and published wind-based empirical relationships to assess the variability of these models (Fig. 4a, Table 1). The relative standard deviation of the mean k_{600} across all wind speeds revealed that k_{600} model variability was greatest at low wind speeds, ranging from 123 % across models when U_{10} = 0.33 m s^{-1} to 50.9 % when U_{10} = 3.50 m s-^{1} (Fig. 4b). k_{600} model variability was lowest when U_{10} ranged from 7.0 – 11.1 m s^{-1}, and the minimum relative standard deviation (18.3 %) occurred when U_{10} = 9.36 m s^{-1} (Fig. 4b).

https://doi.org/10.5194/egusphere-2026-4232
Preprint. Discussion started: 4 August 2026
© Author(s) 2026. CC BY 4.0 License.

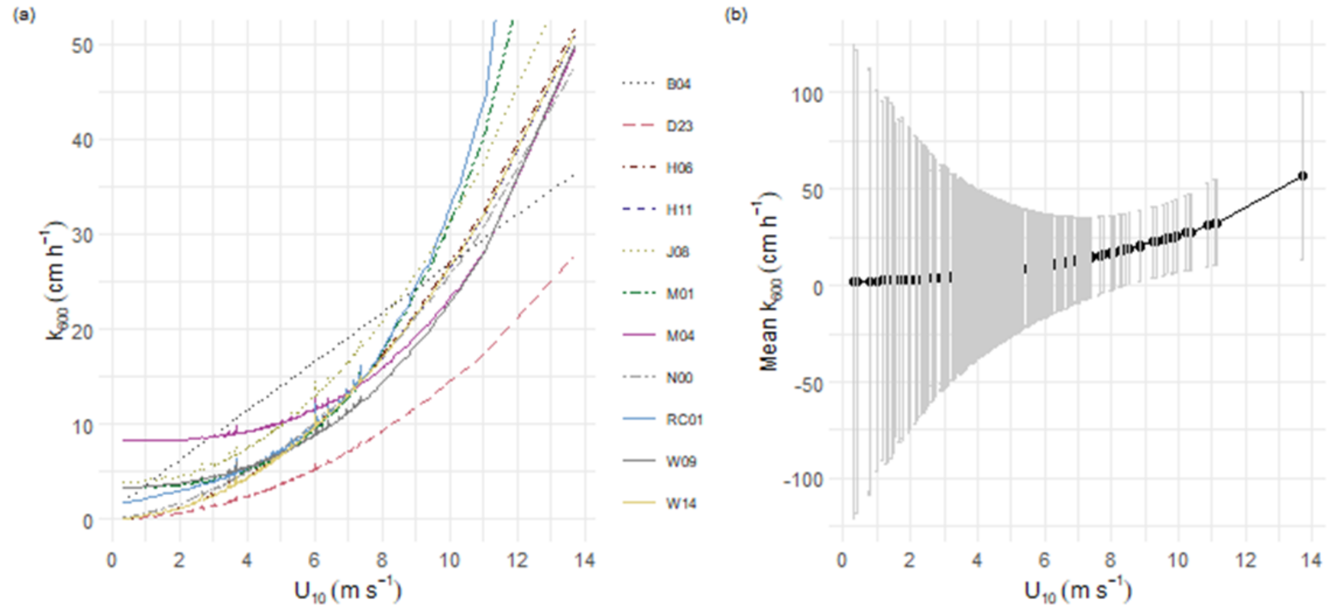

Figure 4: (a) *In situ* U_{10} measurements and eleven published k_{600} models were used to derive *in situ* k_{600} values for SB-152 during the peak seagrass density period. (b) The relative standard deviation of the mean k_{600} value across measured U_{10}. For model equations, see Table 1.

3.2.2 *In situ* gas transfer velocity estimates

In situ k_{O_2} values were derived over SB-152 from high-quality air-water O_2 fluxes produced using the UAEC technique for four hours in 2021 (26 August 2021, 02:45 – 06:45 EDT). During this deployment, the mean wind speed measured at the Rappahannock Light station was U_{10} = 3.03 ± 0.63 m s^{-1} (mean ± SD). Current velocity decreased throughout the deployment and had a mean value of 4.90 ± 2.22 cm s^{-1} (mean ± standard deviation) (Fig. 5a). The deployment occurred during low tide, and the mean water depth was 0.87 ± 0.0082 m (mean ± standard deviation). The water column O_2 concentration ([O_2]) decreased during the deployment (Fig. 5b). The O_2 flux was negative throughout the deployment, showing that the water column was a net sink of O_2 (Fig. 5c). The gas transfer velocity of O_2 (k_{O_2}) decreased with decreasing current velocity throughout the deployment, indicating a positive correlation between current velocity and k_{O_2}(Fig. 5a, 5e). Similarly, a positive correlation between wind speed and current velocity (r = .64, p = .0055, n = 17) was identified with a Spearman's rank-order correlation test using the Hmisc R package (v5.1-1, Harrell, 2023).

https://doi.org/10.5194/egusphere-2026-4232
Preprint. Discussion started: 4 August 2026
© Author(s) 2026. CC BY 4.0 License.

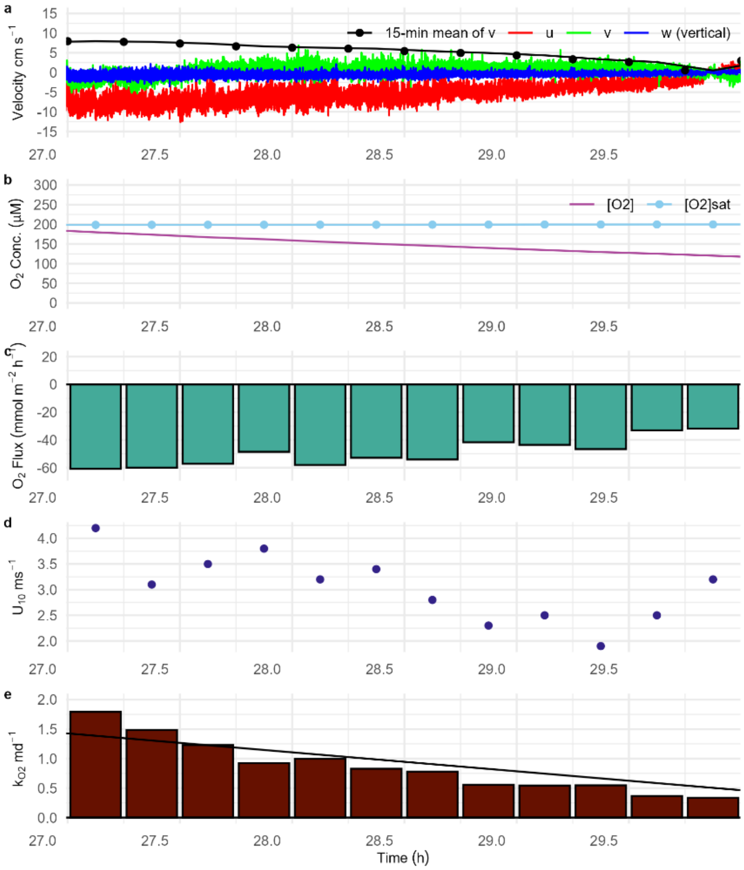

Figure 5: (a) Current velocity measured in three directions (u, v, and w) and the mean current velocity (vmean), as well as (b) water column O_2 concentrations ($[O_2]$) and percent O_2 saturations ($[O_2]_{sat}$), were measured with the upside-down aquatic eddy covariance technique and used to derive (c) 15-minute air-water O_2 fluxes. Negative values represent uptake by the water column. (d) Wind speeds measured at the Rappahannock station and converted to U_{10}. See Figure 1 for wind station location. (e) The gas transfer velocity of O_2 (k_{O_2}) was derived from the O_2 fluxes.

3.2.3 Comparison of *in situ* k_{600} values with modeled values

When the k_{O_2} values derived from the UAEC deployment were converted to k_{600}, simple linear regressions showed that wind speed explained 59 % of the variation in k_{600} and current velocity explained 81% of the variation. The *in situ* k_{600} values ranged from 1.08 cm h^{-1} to 5.71 cm h^{-1} and had a mean value of 2.64 ± 1.46 cm h^{-1} (mean ± standard deviation) (Fig. 6a). The uneven line produced by plotting the *in situ* k_{600} values against wind speed indicated that other variables, such as current velocity and water depth, also partially drove variations in k_{600} at our site (Fig. 6a).

Modeled k_{600} values were also derived for this deployment using established empirical parameterizations (Fig. 6a, Table 1). These empirical parameterizations include the eleven wind-based empirical parameterizations derived from wind speeds

https://doi.org/10.5194/egusphere-2026-4232
Preprint. Discussion started: 4 August 2026
© Author(s) 2026. CC BY 4.0 License.

measured at Rappahannock Light, one empirical parameterization based on current velocity and water depth measured by the UAEC system, and two empirical parameterizations that included wind speed, current velocity, and water depth (Table 1). A Kruskal-Wallis rank-sum test using the R stats package identified significant differences between the k_{600} models (chi-squared = 203.97, p = 2.2 * 10^{-16}) (v4.3.2, R Core Team, 2023). Pairwise Wilcoxon rank-sum tests conducted with the stats R package revealed that the k_{600} values derived from *in situ* data were not significantly different from those calculated by the following wind-based empirical parameterizations: Nightingale et al. (2000) (N00, p = 0.14), Ho et al. (2006) (H06, p = 0.88), Ho et al. (2011) (H11, p = 0.92), and Wanninkhof (2014) (W14, p = 0.92) (n = 17) (v4.3.2, R Core Team, 2023). While the models that included current velocity and water depth (B04c, B04a, and H16) replicated the variability in our *in situ* data, they consistently over-estimated the magnitude (Fig. 6a, Table 1).

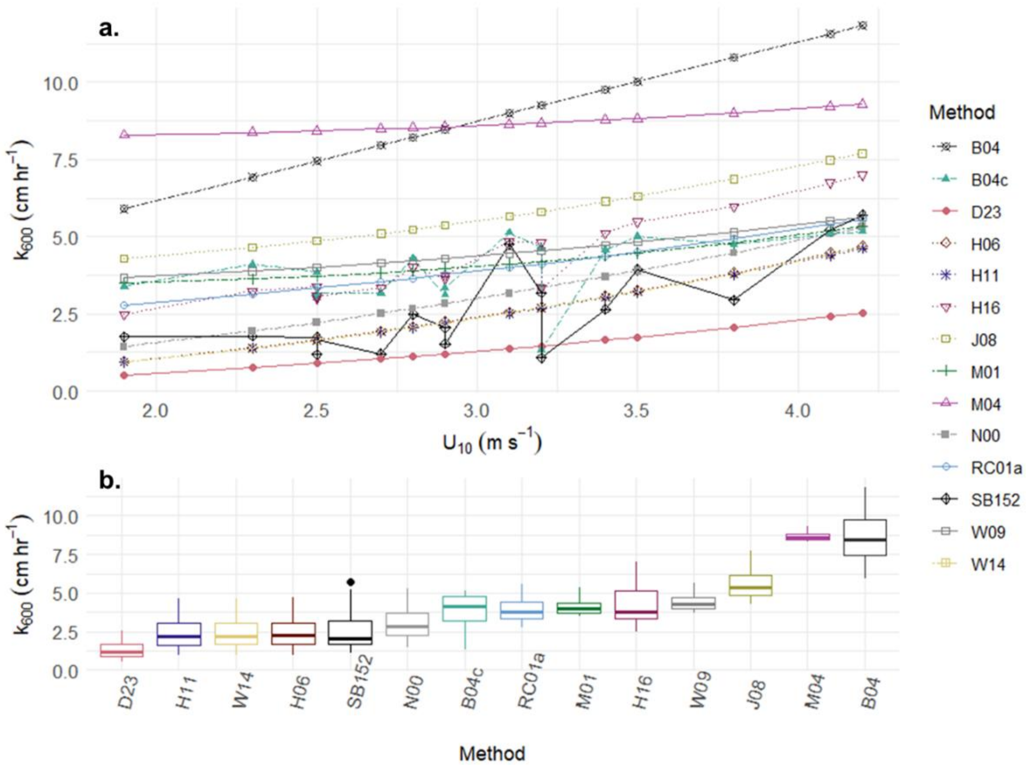

Figure 6: (a) k_{600} values derived from *in situ* data measured during the UAEC deployment plotted with k_{600} values calculated from established empirical parameterizations and *in situ* environmental data. (b) The mean and relative standard deviation of the k_{600} models across deployment wind speeds. The method described by each abbreviation is given in Table 1. The *in situ* k_{600} values are denoted by the code "SB152".

The relative root-mean-square-error (rRMSE) between the *in situ* k_{600} values and each k_{600} model was derived using the Metrics R package (v0.1.4, Hamner and Frasco, 2018), where a lower rRMSE represents a better goodness-of-fit of the model (Table 1) (Ho et al., 2011, 2016). The rRMSE results are in agreement with the results of the rank-sum tests. The four best-fitting

https://doi.org/10.5194/egusphere-2026-4232
Preprint. Discussion started: 4 August 2026
© Author(s) 2026. CC BY 4.0 License.

models had the lowest rRMSE values. The parameterization with the highest rRMSE value included all three environmental variables (wind speed, current velocity, and water depth).

3.3 Diurnal CO_2 fluxes over South Bay

3.3.1 CO_2 flux time series

Of the four best-fitting k_{600} models identified, we selected the Nightingale et al. (2000) model for the purposes of deriving diurnal CO_2 fluxes in this study because this parameterization considered local measurements in fetch-limited environments. Hourly CO_2 fluxes ranged from -2.00 mmol m^{-2} h^{-1} to 5.51 mmol m^{-2} h^{-1} and had a mean value of -0.01 ± 0.842 mmol m^{-2} h^{-1} (mean ± standard deviation), where negative fluxes represent uptake by the water column and positive fluxes represent emission by the water column (Fig. 7a). Mean wind speeds were U_{10} = 4.95 ± 2.01 m s^{-1} (mean ± standard deviation) (Fig. 3). Water column p_{CO_2} concentrations and temperatures exhibited a negative relationship across all years. Changes in the flux magnitude generally followed the sinusoidal pattern of water column pCO_2 and the inverse of the sinusoidal patterns of water column temperature and dissolved O_2 (Fig. 7). The mean k_{CO_2} value was 11.1 ± 7.36 cm h^{-1} (mean ± standard deviation).

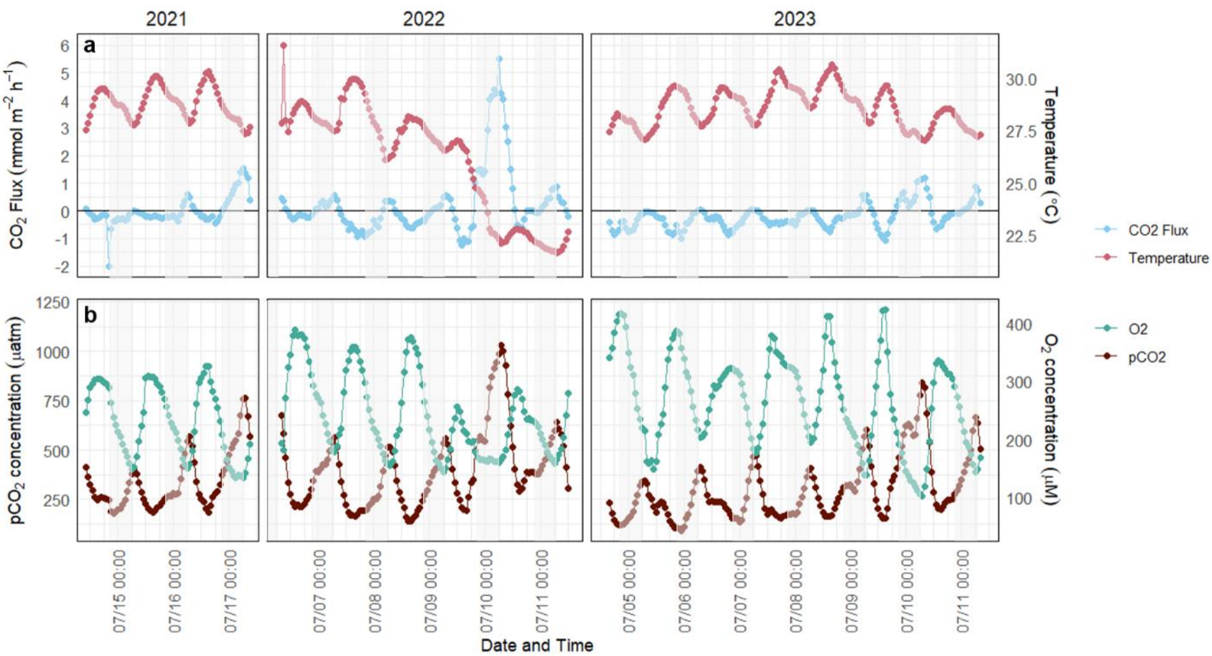

Figure 7: Hourly time series data of (a) CO_2 fluxes, water column temperatures, (b) water column pCO_2 concentrations, and water column O_2 concentrations during the peak seagrass density deployments that occurred in July of 2021, 2022, and 2023. The time of "00:00" on the x axis denotes midnight of each day. Negative CO_2 fluxes represent an uptake of CO_2 by the water column. Gray shading represents nighttime.

https://doi.org/10.5194/egusphere-2026-4232
Preprint. Discussion started: 4 August 2026
© Author(s) 2026. CC BY 4.0 License.

3.3.2 2022 storm period

A storm surge occurred in 2022 from July 9th at 15:00 to July 10th at 08:00 (Fig. 7a). This "storm period" was defined as the period of time where the difference between the predicted astronomical tide and the measured water level at the Wachapreague station was >0.2 m (NOAA NDBC WAHV2) (Zhu and Wiberg, 2022; Castagno et al., 2018). During the storm period, flux magnitudes were approximately 2-5 times greater than the average flux and reached the maximum positive CO_2 flux value (CO_{2max} = 5.51 mmol m^{-2} h^{-1}) (Fig. 7a). The demonstrated sinusoidal pattern in water column temperature was disrupted, and temperatures decreased from 26.70 °C to 21.7 °C, which was the minimum value recorded (Fig. 7a). pCO_2 concentrations increased and reached the maximum value (pCO_{2max} = 1032 µatm) that was well above the average pCO_2 value of 342 ± 176 µatm (mean ± standard deviation) (Fig. 7b). Wind speeds also increased during the storm period (Fig. 3) and reached its maximum value (U_{10max}) of 11.1 m s^{-1}. The maximum negative CO_2 flux (CO_{2min} = -2.00 mmol m^{-2} h^{-1}) occurred on July 14th, 2021, at 20:00 EDT due to a high wind event that occurred within one hour (U_{10} = 13.70 ± 2.40 m s^{-1}, mean ± standard deviation). The increased negative flux likely did not persist because there were no noticeable changes in other variables that were used to derive the flux, such as water column pCO_2 concentrations and temperature (Eq. 5, Fig. 7).

3.3.3 Relationship between hourly average CO_2 fluxes and PAR

All hourly CO_2 fluxes were binned by the hour of the day (Fig. 8). Fluxes followed a diurnal sink-source cycle where South Bay was a source of CO_2 from 01:00 – 11:00 EDT and a sink of CO_2 from 11:00 – 24:00 EDT (Fig. 8). The maximum positive average CO_2 flux was 0.82 mmol CO_2 m^{-2} h^{-1} and occurred at 06:00 EDT, corresponding with the hour in which PAR increased from 0 (Fig. 8). As PAR increased from 06:00 to 10:00 EDT, the positive average CO_2 flux decreased. When the maximum PAR values occurred at 11:00 and 12:00 EDT, the average CO_2 flux switched from positive to negative. The maximum negative average CO_2 flux occurred between 14:00 – 17:00 EDT and was -0.5 mmol CO_2 m^{-2} h^{-1} (Fig. 8). Average PAR decreased to 0 during the 20:00 EDT hour and the average negative CO_2 flux decreased significantly during the 21:00 EDT hour. The significant decrease in the negative flux magnitude one hour after last light (21:00) is partially attributed to the high negative flux (-0.66 mmol CO_2 m^{-2} d^{-1}) that occurred for one hour in 2021 and to the 2022 storm, which primarily occurred overnight (Fig. 7). The cumulative daily sum was -0.60 mmol CO_2 m^{-2} d^{-1}.

https://doi.org/10.5194/egusphere-2026-4232
Preprint. Discussion started: 4 August 2026
© Author(s) 2026. CC BY 4.0 License.

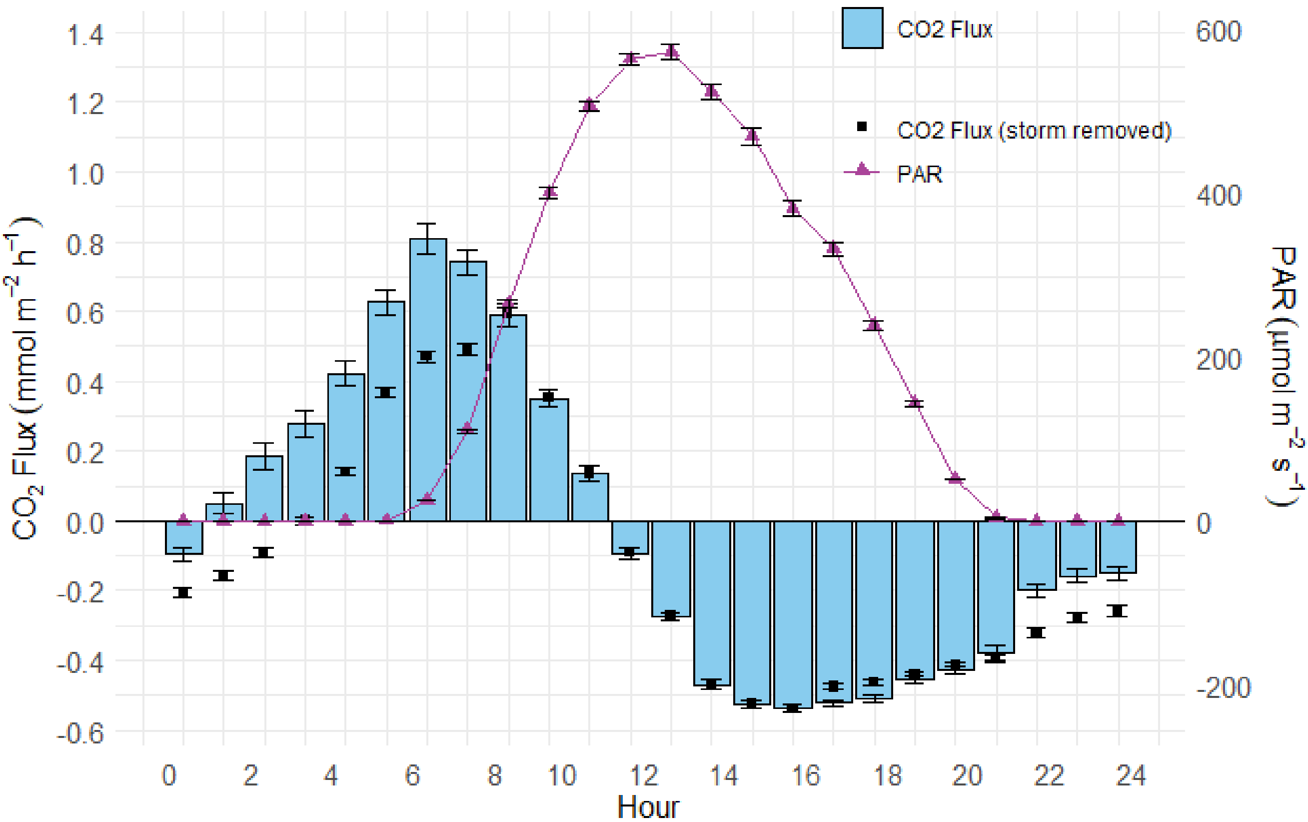

355

Figure 8: CO_2 fluxes and PAR values across all three deployments binned into hourly averages (mean ± SE). To determine the effect of the 2022 storm on the dataset, the CO_2 flux data were also plotted with the storm removed. Negative CO_2 fluxes represent an uptake of CO_2 by the water column.

3.3.4 CO_2 flux variations between stormy and fair-weather periods

360 To assess the effect of storms on the CO_2 flux, we compared the full dataset of hourly average CO_2 fluxes to a dataset with the 2022 storm period removed (Fig. 7, Fig. 8). Without the storm period, the data followed a similar diurnal source-sink cycle as the full dataset, but the magnitude and duration of the negative CO_2 flux was greater (Fig. 8). The magnitude of the positive CO_2 flux was significantly smaller (Fig. 8). The cumulative daily sum of the dataset with the storm period removed was -4.20 mmol CO_2 m^{-2} d^{-1}, significantly overestimating the CO_2 sink capacity of South Bay compared to the full dataset.

https://doi.org/10.5194/egusphere-2026-4232
Preprint. Discussion started: 4 August 2026
© Author(s) 2026. CC BY 4.0 License.

4 Discussion

4.1 Selection of regional wind stations for shallow coastal bays

Wind speeds measured at stations located at or near a land-water interface are often assumed to be representative of estuarine waters, even though the surface roughness over land is greater than over water due to shear stress from land and vegetation (Lawson et al., 2007; Mariotti et al., 2018). Here, wind speeds measured over a barrier island (Hog), a channel (Wachapreague), and at the land-water interface (Kiptopeke) consistently underestimated wind speeds measured over SB-152 by compact anemometer mounted approximately 2.5 m above the sediment surface (Fig. 1, Fig 3). Similar results were reported in the Mississippi Delta estuary, where the underestimation of bay wind speeds by land stations was greatest when the winds were originating from land (Mariotti et al., 2018). To appropriately represent wind speeds over bays such as South Bay with land stations, a boundary layer correction is needed when the wind comes from the direction of land (Hsu, 1986; Schwing and Blanton, 1984). This is particularly important for gas exchange estimates because the relationship between wind speed and gas transfer velocity (k) is generally reported with a quadratic or power function, so an underestimation in wind speeds for example would result in a significant underestimation of k and result in an underestimation of the derived gas flux (Eq. 5). Ultimately, a bias in the wind speed of ≥ 1 m s^{-1} can bias the CO_2 flux by 43% or in some cases even greater (Wanninkhof et al., 2002, 2009).

Wind speeds measured at Rappahannock Light, the wind station located offshore in the Chesapeake Bay, were not significantly different to those measured over SB-152 (Fig. 1, Fig. 3). Wind speed estimates derived offshore of the Chesapeake Bay with the ERA-5 analysis were also not significantly different from the *in situ* station or from Rappahannock Light in this study (Fig. 3, Zhu et al. *in prep*). Overall, our study suggest that regional wind stations located over water or fine-scale models such as the ERA-5 reanalysis provide the most appropriate estimates of wind speeds over shallow coastal bays. Regional wind states located on or near land are not always representative of offshore estuarine waters.

4.2 Best fitting parameterizations for South Bay

Recently, there has been an enhanced effort to constrain gas transfer velocities in estuaries (Van Dam et al., 2019; Rosentreter et al., 2021; Dobashi and Ho, 2023). Different empirical wind speed parameterizations can produce highly variable k_{600} values in estuaries, partially because of the lack of observational data over the ocean when $U_{10} < 4$ m s^{-1}, a value that estuarine wind speeds are often at or below (Wanninkhof et al., 2009; Dobashi and Ho, 2023; Ho et al., 2018). This is particularly relevant for selecting a k_{600} model for our study because $U_{10} \leq 5$ m s^{-1} for 60 % of the total period of our CO_2 flux estimates (Fig. 6, Fig. 7). We observed the most variability in k_{600} values produced by the wind speed parameterizations when $U_{10} \leq 5$ m s^{-1} (Fig. 4b).

In other vegetated estuaries, variability in k_{600} values indicated that gas transfer velocity was attributed to multiple drivers of gas exchange beyond wind speed, such as current velocity and water depth (Ho et al., 2016; Rosentreter et al., 2017). Thus, we evaluated parameterizations that included current velocity and water depth (B04c, B04a, H16) in addition to the wind speed

https://doi.org/10.5194/egusphere-2026-4232
Preprint. Discussion started: 4 August 2026
© Author(s) 2026. CC BY 4.0 License.

parameterizations during the k_{600} model analysis (Fig. 6, Table 1). The current velocity and water depth parameterizations captured the *in situ* k_{600} variability, but consistently over-estimated the magnitude (Fig. 6). This may be because wind-driven small waves, ripples, and currents are the dominant forcing in South Bay, which means that wind speed and current velocity are correlated (Lawson et al., 2007; Fagherazzi and Wiberg, 2009). Due to this correlation, including both wind speed and velocity in parameterizations may overestimate the gas transfer velocity at our site. The ability to ground-truth site-specific k_{600} values using the UAEC technique was critical in determining which models were the best fit for our site.

We determined that there were four models that fit our site best because they produced k_{600} values that were not significantly different from the *in situ* values: Nightingale et al. (2000), Ho et al. (2006), Ho et al. (2011), and Wanninkhof et al. (2014) (Table 1, Fig. 5). We chose Nightingale et al. (2000) (N00) as the empirical parameterization for our CO_2 flux estimates because this parameterization considered local measurements in fetch-limited environments. Wanninkhof (2014) (W14), a widely used model, was also one of our best fitting models. We selected N00 over W14 because W14 was recommended for regional to global wind speed estimates of *k*. Our analysis was limited to low and low-intermediate wind speeds.

Ultimately, the best fitting models in our study (N00, H06, H11, and W14) were wind speed parameterizations that were derived over the ocean and had an intercept of zero (Fig. 6, Table 1). Our results are in agreement with another study conducted in a tidal river estuary that found that parameterizations derived from the open ocean with an intercept of zero were better predictors of k_{600} compared to parameterizations derived over estuaries or over the ocean with a nonzero intercept (Ho et al., 2016). In our study, the parameterizations with nonzero intercepts derived over either the open ocean (M01, M04, J08, and W09) or estuaries (R01 and B04) overestimated k_{600} at the low wind speeds in our study, although the curves of M01 and W09 suggest that they may better predict k_{600} over South Bay when $U_{10} \geq 5$ m s^{-1} (Fig. 6). This may be due to the influence of current velocity on gas transfer velocity at our site (Wanninkhof et al., 2009; Ho et al., 2016).

Surprisingly, k_{600} was consistently underestimated by an empirical wind speed parameterization derived over a different seagrass meadow (D23) (Dobashi and Ho, 2023). The Dobashi and Ho (2023) parameterization was determined in April in a meadow where the dominant seagrass was *Thalassia testudinum*, so this underestimation could be due to differences in site-specific environmental conditions, such as seagrass density. High seagrass densities are known to attenuate flow, and it is possible that their parameterization may fit our site better either before or during the early growing season (Reidenbach and Thomas, 2018; Zhu et al., 2021). Differences in k_{600} within ecosystems have been reported in mangrove forests, where a uniform k_{600} value derived at one site (Ho et al., 2016) underestimated CO_2 fluxes at a similar site by 33 % on average (Rosentreter et al., 2017). The presence of submerged, floating, and emergent vegetation can similarly affect gas exchange by reducing flows, facilitating direct gas exchange across the sediment-water or plant-water interface, and disrupting the air-water boundary layer (Ho et al., 2018; Zhu et al., 2021).

4.3 Diurnal variability in CO_2 fluxes

Hourly CO_2 fluxes varied in magnitude and direction, demonstrating the rapid internal cycling of C_{inorg} that occurs in seagrass meadows (Fig. 6a) (Yang et al., 2019). The inverse sinusoidal relationship of water column p_{CO_2} and O_2 concentrations shown

https://doi.org/10.5194/egusphere-2026-4232
Preprint. Discussion started: 4 August 2026
© Author(s) 2026. CC BY 4.0 License.

here and in previous work (Berg et al., 2019) suggests that the hourly-scale variability in the CO_2 fluxes is driven by patterns in photosynthesis and respiration (Fig. 6b). The differences between the water column concentration patterns and the variability in the CO_2 flux suggests that a significant amount of this metabolism is occurring in the water column, which is in agreement with the findings of Berg et al. (2019). The time periods in which South Bay was a CO_2 sink primarily occurred during the day, and the time periods in which South Bay was a CO_2 source primarily occurred overnight (Fig. 6, Fig. 7). This suggests that evaluating the CO_2 flux during the daytime only will overestimate the total CO_2 sink capacity of seagrass meadow ecosystems. We find that these patterns are interannually persistent, except for during the storm period. Averaged over all deployments, the hourly CO_2 fluxes followed a diurnal source-sink pattern with PAR and the cumulative daily sum was -0.60 mmol CO_2 m^{-2} d-1, indicating that South Bay, the seagrass meadow and the water column above, is in metabolic balance during peak seagrass density, despite being a larger source of CO_2 during storms (Fig. 7). Our results are in line with an analysis of decadal ecosystem metabolism in South Bay determined from benthic O_2 fluxes that found similarly that the seagrass meadow was in metabolic balance (Berger et al., 2020).

4.4 Effect of storms on CO_2 fluxes

A storm surge occurred during the July 2022 deployment, which was identified as a period of time where the difference between the predicted astronomical tide and the measured water level at the Wachapreague station was > 0.2 m (NOAA NDBC WAHV2) (Zhu and Wiberg, 2022; Castagno et al., 2018). During this storm surge period, there was a decrease in water temperature, an increase in water column pCO_2 concentrations, and an increase in wind speed that was documented *in situ* over South Bay, at the Rappahannock Light station, and in the ERA-5 reanalysis (Fig. 3, Fig. 7). To a lesser extent, the Wachapreague station, the Kiptopeke station, and the Hog stations showed a wind speed increase during this time, likely due to the dampening effects of land (Fig. 3). Further, the maximum positive CO_2 flux recorded in this study occurred during this storm period (Fig. 6a). By measuring all components of the flux equation (Eq. 5) on temporal scales ≤ 1 min, we captured the effect of rapid changes in k_{CO_2} from wind speed, K_0 from temperature, and ΔpCO_2 from water column pCO_2 on the CO_2 flux (Fig. 6).

The maximum negative CO_2 flux recorded in this study occurred in 2021 when the mean wind speed was U_{10} = 13.70 ± 2.40 m s^{-1}, but this flux did not persist for more than an hour and no significant change in temperature was measured. Similarly, we did not identify a storm surge during this period, so this flux was not included as a storm period.

When the 2022 storm was removed from the dataset, the dataset overestimated the daily CO_2 sink capacity of South Bay (Fig. 7, Fig. 8). Effects of storms in particular are not well-documented in existing CO_2 flux measurements over estuaries. Storm events over the VCR occurred for 5 % of the total time between August 2008 to December 2020, but storm events may increase in the future due to the potential effects of sea level rise and potential changes to the intensity and frequency of storms from changes in our climate (Zhu and Wiberg, 2022; Kulp and Strauss, 2019; Lin et al., 2019). During storm periods, there is increased resuspension of suspended sediments that may facilitate increased gas exchange from the sediment to the water column and then to the atmosphere (Zhu and Wiberg, 2024; Zhu et al., 2021). Increased wind speeds, whitecapping, bubble entrainment, and rainfall may also contribute to a thinning of the air-water boundary layers, further facilitating gas exchange (Wanninkhof et al., 2009; Ho et al., 2000). The relationship between wind speed and gas exchange should be studied further during storm periods to better constrain the effect of these variables on gas fluxes.

5 Conclusions

Measuring air-water CO_2 fluxes on fine temporal scales is essential for disentangling diurnal and inter-annual patterns. In this study, we performed a regional wind speed analysis, an analysis of *in situ* and modeled k_{600} values, and a long-term study of diurnal CO_2 flux patterns over South Bay, a shallow coastal bay with a temperate seagrass meadow dominating the benthos. The regional wind speed station that gave measurements closest to those recorded at our site was located in the Chesapeake Bay. All stations located in proximity to land underestimated wind speeds over South Bay, which would ultimately underestimate the k_{600} value, and thus, the CO_2 flux. The results of the analysis of *in situ* and modeled k_{600} values determined that the best fitting k_{600} models were wind speed parameterizations that were derived over the open ocean and that had an intercept of zero. In estuaries, the most appropriate k_{600} model is likely site-specific and should be determined using *in situ* k_{600} data when possible, or alternatively, by thoroughly evaluating site characteristics such as water depth, current velocity, and wind speed. We applied the regional wind speed analysis and the k_{600} model analysis and derived air-water hourly CO_2 fluxes during the peak seagrass density period (early July) for three years. The magnitude and direction of the CO_2 flux varied on hourly and diurnal time scales, but the daily average showed that South Bay was in metabolic balance and was a minor CO_2 sink. This study captured a storm period in 2022. South Bay was a clear source of CO_2 during the storm period. Storm events occurred approximately 5 % of the time at our site, and should be taken into account when evaluating CO_2 fluxes over estuaries on broad temporal and spatial scales.

Code availability

The code that support the findings of this study are available from the corresponding author upon request.

Data availability

The data that support the findings of this study are available from the corresponding author upon request.

Author Contributions

KEG and PB designed the diurnal CO_2 flux evaluation and KEG conducted the fieldwork, labwork, and data analysis. PB designed the upside-down aquatic eddy covariance system and carried out of the testing. KEG designed and carried out the regional wind analysis. KEG prepared the manuscript with contributions from PB.

© Author(s) 2026. CC BY 4.0 License.

Competing interests

The authors declare that they have no conflict of interest.

Acknowledgements

Support for this study was provided by the University of Virginia and the National Science Foundation through the following grants: the Virginia Coast Reserve Long-Term Ecological Research Program (DEB-1832221, DEB-2425178), to Peter Berg (OCE-2223204), and to Kayleigh Granville through the Virginia Sea Grant Graduate Research Fellowship and the Jefferson Scholars Foundation Dissertation Year Fellowship. The research was conducted at and supported by resources available through the University of Virginia's Anheuser-Busch Coastal Research Center, located at the Virginia Coast Reserve Long-Term Ecological Research site. We thank the staff at the University of Virginia's Anheuser-Busch Coastal Research Center, as well as Ieva Juska, Carly LaRoche, Meg Miller, and Luke Groff for their assistance in the field and lab. We also thank Scott Doney, Carly LaRoche, Patricia Wiberg, and Qingguang Zhu for their feedback that improved this study.

References

Aoki, L. R., McGlathery, K. J., Wiberg, P. L., Oreska, M. P. J., Berger, A. C., Berg, P., and Orth, R. J.: Seagrass Recovery Following Marine Heat Wave Influences Sediment Carbon Stocks, Front Mar Sci, 7, https://doi.org/10.3389/fmars.2020.576784, 2021.

Berg, P. and Pace, M. L.: Continuous measurement of air-water gas exchange by underwater eddy covariance, Biogeosciences, 14, 5595–5606, https://doi.org/10.5194/bg-14-5595-2017, 2017.

Berg, P., Roy, H., Janssen, F., Meyer, V., Jorgensen, B. B., Huettel, M., and de Beer, D.: Oxygen uptake by aquatic sediments measured with a novel non-invasive eddy-correlation technique, Mar Ecol Prog Ser, 261, 75–83, 2003.

Berg, P., Delgard, M. L., Glud, R. N., Huettel, M., Reimers, C. E., and Pace, M. L.: Non-invasive Flux Measurements at the Benthic Interface: The Aquatic Eddy Covariance Technique, Limnology and Oceanography e-Lectures, https://doi.org/10.1002/loe2.10005, 2017.

Berg, P., Delgard, M. L., Polsenaere, P., McGlathery, K. J., Doney, S. C., and Berger, A. C.: Dynamics of benthic metabolism, O 2 , and pCO 2 in a temperate seagrass meadow , Limnol Oceanogr, https://doi.org/10.1002/lno.11236, 2019.

Berg, P., Pace, M. L., and Buelo, C. D.: Air–water gas exchange in lakes and reservoirs measured from a moving platform by underwater eddy covariance, Limnol Oceanogr Methods, lom3.10373, https://doi.org/10.1002/lom3.10373, 2020.

Berg, P., Huettel, M., Glud, R. N., Reimers, C. E., and Attard, K. M.: Aquatic Eddy Covariance: The Method and Its Contributions to Defining Oxygen and Carbon Fluxes in Marine Environments, Ann Rev Mar Sci, 14, 431–455, https://doi.org/10.1146/annurev-marine-042121-012329, 2022.

Berg, P., Hebert, R.M., McKenzie, M.A., Groff, L.D., Wiman, C., Garneau, P., Gould, J., Kuzminski, S., McGlathery, K.J., Muñoz, S., Hughes, A.R., Stubbins, A., and Miller, L.E.: Century-scale resilience of stored seagrass blue carbon. Limnol Oceanogr Letters, 10, 990-998, doi: 10.1002/lol2.70056, 2025.

Berger, A. C., Berg, P., McGlathery, K. J., and Delgard, M. L.: Long-term trends and resilience of seagrass metabolism: A decadal aquatic eddy covariance study, Limnol Oceanogr, https://doi.org/10.1002/lno.11397, 2020.

https://doi.org/10.5194/egusphere-2026-4232
Preprint. Discussion started: 4 August 2026
© Author(s) 2026. CC BY 4.0 License.

Berger, A. C., Berg, P., Mcglathery, K., Reidenbach, M. A., Pace, M. L., and Goodall, J. L.: Long-term aquatic eddy covariance measurements of seagrass metabolism and ecosystem response to warming oceans, 2021.

Bianchi, T. S., Cui, X., Blair, N. E., Burdige, D. J., Eglinton, T. I., and Galy, V.: Centers of organic carbon burial and oxidation at the land-ocean interface, https://doi.org/10.1016/j.orggeochem.2017.09.008, 1 January 2018.

Borges, A. V., Abril, G., and Bouillon, S.: Carbon dynamics and CO2 and CH4 outgassing in the Mekong delta, Biogeosciences, 15, 1093–1114, https://doi.org/10.5194/bg-15-1093-2018, 2018.

Castagno, K. A., Jiménez-Robles, A. M., Donnelly, J. P., Wiberg, P. L., Fenster, M. S., and Fagherazzi, S.: Intense Storms Increase the Stability of Tidal Bays, Geophys Res Lett, 45, 5491–5500, https://doi.org/10.1029/2018GL078208, 2018.

Cheng, J., Schloerke, B., Karambelkar, B., Xie, Y.: _leaflet: Create Interactive Web Maps with the JavaScript 'Leaflet' Library_. R packageversion 2.2.2, <https://CRAN.R-project.org/package=leaflet>, 2024.

Cole, J. J., Bade, D. L., Pace, M. L., and Van de Bogert, M.: Multiple approaches to estimating air-water gas exchange in small lakes., 2010.

Copernicus Climate Change Service (): <2023>. Complete ERA5 global atmospheric reanalysis. Copernicus Climate Change Service (C3S) Climate Data Store (CDS). DOI: 10.24381/cds.143582cf (Accessed on 21-02-2024)

Van Dam, B. R., Edson, J. B., and Tobias, C.: Parameterizing Air-Water Gas Exchange in the Shallow, Microtidal New River Estuary, J Geophys Res Biogeosci, 124, 2351–2363, https://doi.org/10.1029/2018JG004908, 2019.

Van Dam, B., Polsenaere, P., Barreras-Apodaca, A., Lopes, C., Sanchez-Mejia, Z., Tokoro, T., Kuwae, T., Loza, L. G., Rutgersson, A., Fourqurean, J., and Thomas, H.: Global Trends in Air-Water CO2 Exchange Over Seagrass Meadows Revealed by Atmospheric Eddy Covariance, Global Biogeochem Cycles, 35, https://doi.org/10.1029/2020GB006848, 2021.

Dobashi, R. and Ho, D. T.: Air–sea gas exchange in a seagrass ecosystem – results from a $^{3}He/SF_{6}$ tracer release experiment, Biogeosciences, 20, 1075–1087, https://doi.org/10.5194/bg-20-1075-2023, 2023.

Fagherazzi, S. and Wiberg, P. L.: Importance of wind conditions, fetch, and water levels on wave-generated shear stresses in shallow intertidal basins, J Geophys Res Earth Surf, 114, https://doi.org/10.1029/2008JF001139, 2009.

Fennel, K., Alin, S., Barbero, L., Evans, W., Bourgeois, T., Cooley, S., Dunne, J., Feely, R. A., Martin Hernandez-Ayon, J., Hu, X., Lohrenz, S., Muller-Karger, F., Najjar, R., Robbins, L., Shadwick, E., Siedlecki, S., Steiner, N., Sutton, A., Turk, D., Vlahos, P., and Aleck Wang, Z.: Carbon cycling in the North American coastal ocean: A synthesis, Biogeosciences, 16, 1281–1304, https://doi.org/10.5194/bg-16-1281-2019, 2019.

Frankignoulle, M. and Borges, A. V.: European continental shelf as a significant sink for atmospheric carbon dioxide, Global Biogeochem Cycles, 15, 569–576, https://doi.org/10.1029/2000GB001307, 2001.

Garcia, H. and Gordon, L.: Oxygen Solubility in Seawater: Better Fitting Equations, Limnol Oceanogr, 37, 1307–1312, 1992.

Gattuso J, Epitalon J, Lavigne H, Orr J (2024). _seacarb: Seawater Carbonate Chemistry_. R package version 3.3.3, <https://CRAN.R-project.org/package=seacarb>.

Granville, K. E., Berg, P., and Huettel, M.: A high-resolution submersible oxygen optode system for aquatic eddy covariance, Limnol Oceanogr Methods, 21, 152–163, https://doi.org/10.1002/lom3.10535, 2023.

https://doi.org/10.5194/egusphere-2026-4232
Preprint. Discussion started: 4 August 2026
© Author(s) 2026. CC BY 4.0 License.

Hersbach, H., Bell, B., Berrisford, P., Hirahara, S., Horányi, A., Muñoz-Sabater, J., Nicolas, J., Peubey, C., Radu, R., Schepers, D., Simmons, A., Soci, C., Abdalla, S., Abellan, X., Balsamo, G., Bechtold, P., Biavati, G., Bidlot, J., Bonavita, M., De Chiara, G., Dahlgren, P., Dee, D., Diamantakis, M., Dragani, R., Flemming, J., Forbes, R., Fuentes, M., Geer, A., Haimberger, L., Healy, S., Hogan, R.J., Hólm, E., Janisková, M., Keeley, S., Laloyaux, P., Lopez, P., Lupu, C., Radnoti, G., de Rosnay, P., Rozum, I., Vamborg, F., Villaume, S., Thépaut, J-N. (2017): Complete ERA5 from 1940: Fifth generation of ECMWF atmospheric reanalyses of the global climate. Copernicus Climate Change Service (C3S) Data Store (CDS). DOI: 10.24381/cds.143582cf (Accessed on 21-02-2024)

Ho, D. T., Asher, W. E., Bliven, L. F., Schlosser, P., and Gordan, E. L.: On mechanisms of rain-induced air-water gas exchange, J Geophys Res Oceans, 105, 24045–24057, https://doi.org/10.1029/1999jc000280, 2000.

Ho, D. T., Law, C. S., Smith, M. J., Schlosser, P., Harvey, M., and Hill, P.: Measurements of air-sea gas exchange at high wind speeds in the Southern Ocean: Implications for global parameterizations, Geophys Res Lett, 33, https://doi.org/10.1029/2006GL026817, 2006.

Ho, D. T., Wanninkhof, R., Schlosser, P., Ullman, D. S., Hebert, D., and Sullivan, K. F.: Toward a universal relationship between wind speed and gas exchange: Gas transfer velocities measured with 3He/SF6 during the Southern Ocean Gas Exchange Experiment, J Geophys Res Oceans, 116, https://doi.org/10.1029/2010JC006854, 2011.

Ho, D. T., Coffineau, N., Hickman, B., Chow, N., Koffman, T., and Schlosser, P.: Influence of current velocity and wind speed on air-water gas exchange in a mangrove estuary, Geophys Res Lett, 43, 3813–3821, https://doi.org/10.1002/2016GL068727, 2016.

Ho, D. T., Engel, V. C., Ferrón, S., Hickman, B., Choi, J., and Harvey, J. W.: On Factors Influencing Air-Water Gas Exchange in Emergent Wetlands, J Geophys Res Biogeosci, 123, 178–192, https://doi.org/10.1002/2017JG004299, 2018.

Hsu, S. A.: A Mechanism for the Increase of Wind Stress (Drag) Coefficient with Wind Speed over Water Surfaces: A Parametric Model, J Phys Oceanogr, 16, 144–150, https://doi.org/10.1175/1520-0485(1986)016<0144:AMFTIO>2.0.CO;2, 1986.

Jähne, B., Münnich, K. O., Bösinger, R., Dutzi, A., Huber, W., and Libner, P.: On the parameters influencing air-water gas exchange, J Geophys Res Oceans, 92, 1937–1949, https://doi.org/10.1029/JC092iC02p01937, 1987.

Jeffrey, L. C., Maher, D. T., Santos, I. R., Call, M., Reading, M. J., Holloway, C., and Tait, D. R.: The spatial and temporal drivers of pCO2, pCH4 and gas transfer velocity within a subtropical estuary., Estuar Coast Shelf Sci, 208, 83–95, https://doi.org/10.1016/j.ecss.2018.04.022, 2018.

Kim, S. H., Suonan, Z., Qin, L. Z., Kim, H., Park, J. I., Kim, Y. K., Lee, S., Kim, S. G., Kang, C. K., and Lee, K. S.: Variability in blue carbon storage related to biogeochemical factors in seagrass meadows off the coast of the Korean peninsula, Science of the Total Environment, 813, https://doi.org/10.1016/j.scitotenv.2021.152680, 2022.

Kulp, S. A. and Strauss, B. H.: New elevation data triple estimates of global vulnerability to sea-level rise and coastal flooding, Nat Commun, 10, https://doi.org/10.1038/s41467-019-12808-z, 2019.

Lawson, S. E., Wiberg, P. L., McGlathery, K. J., and Fugate, D. C.: Wind-driven Sediment Suspension Controls Light Availability in a Shallow Coastal Lagoon, Estuaries and Coasts, 30, 102–112, 2007.

Lin, N., Marsooli, R., and Colle, B. A.: Storm surge return levels induced by mid-to-late-twenty-first-century extratropical cyclones in the Northeastern United States, Clim Change, 154, 143–158, https://doi.org/10.1007/s10584-019-02431-8, 2019.

© Author(s) 2026. CC BY 4.0 License.

Long, M. H. and Nicholson, D. P.: Surface gas exchange determined from an aquatic eddy covariance floating platform, Limnol Oceanogr Methods, 16, 145–159, https://doi.org/10.1002/lom3.10233, 2018.

Macreadie, P. I., Costa, M. D. P., Atwood, T. B., Friess, D. A., Kelleway, J. J., Kennedy, H., Lovelock, C. E., Serrano, O., and Duarte, C. M.: Blue carbon as a natural climate solution, Nat Rev Earth Environ, https://doi.org/10.1038/s43017-021-00224-1, 2021.

Mariotti, G., Huang, H., Xue, Z., Li, B., Justic, D., and Zang, Z.: Biased wind measurements in Estuarine waters, J Geophys Res Oceans, 123, 3577–3587, https://doi.org/10.1029/2017JC013748, 2018.

Mcgillis, W. R., Edson, J. B., Ware, J. D., Dacey, J. W. H., Hare, J. E., Fairall, C. W., and Wanninkhof, R.: Carbon dioxide flux techniques performed during GasEx-98, Marine Chemistry, 267–280 pp., 2001.

McGillis, W. R., Edson, J. B., Zappa, C. J., Ware, J. D., McKenna, S. P., Terray, E. A., Hare, J. E., Fairall, C. W., Drennan, W., Donelan, M., DeGrandpre, M. D., Wanninkhof, R., and Feely, R. A.: Air-sea CO2 exchange in the equatorial Pacific, J Geophys Res Oceans, 109, https://doi.org/10.1029/2003JC002256, 2004.

McGlathery, K. J., Reynolds, L. K., Cole, L. W., Orth, R. J., Marion, S. R., and Schwarzschild, A.: Recovery trajectories during state change from bare sediment to eelgrass dominance, Mar Ecol Prog Ser, 448, 209–221, https://doi.org/10.3354/meps09574, 2012.

Mu, L., Stammerjohn, S. E., Lowry, K. E., and Yager, P. L.: Spatial variability of surface pCO2 and air-sea CO2 flux in the Amundsen Sea Polynya, Antarctica, Elementa: Science of the Anthropocene, 2, 000036, https://doi.org/10.12952/journal.elementa.000036, 2014.

Nightingale, P. D., Malin, G., Law, C. S., Watson, A. J., Liss, P. S., Liddicoat, M. I., Boutin, J., and Upstill-Goddard, R. C.: In situ evaluation of air-sea gas exchange parameterizations using novel conservative and volatile tracers, Global Biogeochem Cycles, 14, 373–387, https://doi.org/10.1029/1999GB900091, 2000.

Ollivier, Q. R., Maher, D. T., Pitfield, C., and Macreadie, P. I.: Net Drawdown of Greenhouse Gases (CO2, CH4 and N2O) by a Temperate Australian Seagrass Meadow, Estuaries and Coasts, 45, 2026–2039, https://doi.org/10.1007/s12237-022-01068-8, 2022.

Oreska, M. P. J., McGlathery, K. J., Aoki, L. R., Berger, A. C., Berg, P., and Mullins, L.: The greenhouse gas offset potential from seagrass restoration, Sci Rep, 10, https://doi.org/10.1038/s41598-020-64094-1, 2020.

Orth, R. J., Lefcheck, J. S., Mcglathery, K. S., Aoki, L., Luckenbach, M. W., Moore, K. A., Oreska, M. P. J., Snyder, R., Wilcox, D. J., and Lusk, B.: Restoration of seagrass habitat leads to rapid recovery of coastal ecosystem services, Sci. Adv, 2020.

Prentice, C., Poppe, K. L., Lutz, M., Murray, E., Stephens, T. A., Spooner, A., Hessing-Lewis, M., Sanders-Smith, R., Rybczyk, J. M., Apple, J., Short, F. T., Gaeckle, J., Helms, A., Mattson, C., Raymond, W. W., and Klinger, T.: A Synthesis of Blue Carbon Stocks, Sources, and Accumulation Rates in Eelgrass (Zostera marina) Meadows in the Northeast Pacific, Global Biogeochem Cycles, 34, https://doi.org/10.1029/2019GB006345, 2020.

R Core Team (2024). _R: A Language and Environment for Statistical Computing_. R Foundation for Statistical Computing, Vienna, Austria. <https://www.R-project.org/>.

Reidenbach, M. A. and Thomas, E. L.: Influence of the Seagrass, Zostera marina, on wave attenuation and bed shear stress within a shallow coastal bay, Front Mar Sci, 5, https://doi.org/10.3389/fmars.2018.00397, 2018.

https://doi.org/10.5194/egusphere-2026-4232
Preprint. Discussion started: 4 August 2026
© Author(s) 2026. CC BY 4.0 License.

Rheuban, J. E., Berg, P., and McGlathery, K. J.: Multiple timescale processes drive ecosystem metabolism in eelgrass (Zostera marina) meadows, Mar Ecol Prog Ser, 507, 1–13, https://doi.org/10.3354/meps10843, 2014.

Ricart, A. M., York, P. H., Bryant, C. V., Rasheed, M. A., Ierodiaconou, D., and Macreadie, P. I.: High variability of Blue Carbon storage in seagrass meadows at the estuary scale, Sci Rep, 10, https://doi.org/10.1038/s41598-020-62639-y, 2020.

Rosentreter, J. A., Maher, D. T., Ho, D. T., Call, M., Barr, J. G., and Eyre, B. D.: Spatial and temporal variability of CO2 and CH4 gas transfer velocities and quantification of the CH4 microbubble flux in mangrove dominated estuaries, Limnol Oceanogr, 62, 561–578, https://doi.org/10.1002/lno.10444, 2017.

Rosentreter, J. A., Wells, N. S., Ulseth, A. J., and Eyre, B. D.: Divergent Gas Transfer Velocities of CO2, CH4, and N2O Over Spatial and Temporal Gradients in a Subtropical Estuary, J Geophys Res Biogeosci, 126, https://doi.org/10.1029/2021JG006270, 2021.

Saderne, V., Geraldi, N. R., Macreadie, P. I., Maher, D. T., Middelburg, J. J., Serrano, O., Almahasheer, H., Arias-Ortiz, A., Cusack, M., Eyre, B. D., Fourqurean, J. W., Kennedy, H., Krause-Jensen, D., Kuwae, T., Lavery, P. S., Lovelock, C. E., Marba, N., Masqué, P., Mateo, M. A., Mazarrasa, I., McGlathery, K. J., Oreska, M. P. J., Sanders, C. J., Santos, I. R., Smoak, J. M., Tanaya, T., Watanabe, K., and Duarte, C. M.: Role of carbonate burial in Blue Carbon budgets, Nat Commun, 10, https://doi.org/10.1038/s41467-019-08842-6, 2019.

Schwing, F. B. and Blanton, J. O.: The Use of Land and Sea Based Wind Data in a Simple Circulation Model, J Phys Oceanogr, 14, 193–197, https://doi.org/10.1175/1520-0485(1984)014<0193:TUOLAS>2.0.CO;2, 1984.

Vieira Borges, A., Vanderborght, J.-P., Schiettecatte, L.-S., Dé, F., Gazeau, R., Ferro´n, S., Ferro´n-Smith, F., Delille, B., and Frankignoulle, M.: Variability of the Gas Transfer Velocity of CO 2 in a Macrotidal Estuary (the Scheldt), Estuarine Research Federation Estuaries, 593–603 pp., 2004.

Wanninkhof, R.: Relationship between wind speed and gas exchange over the ocean, J Geophys Res, 97, 7373–7382, https://doi.org/10.1029/92JC00188, 1992.

Wanninkhof, R.: Relationship between wind speed and gas exchange over the ocean revisited, Limnol Oceanogr Methods, 12, 351–362, https://doi.org/10.4319/lom.2014.12.351, 2014.

Wanninkhof, R., Doney, S. C., Takahashi, T., and McGillis, W. R.: The effect of using time-averaged winds on regional air-sea CO2 fluxes, in: Gas transfer at water surfaces, vol. 127, Blackwell Publishing Ltd, 351–356, https://doi.org/10.1029/GM127p0351, 2002.

Wanninkhof, R., Asher, W. E., Ho, D. T., Sweeney, C., and McGillis, W. R.: Advances in Quantifying Air-Sea Gas Exchange and Environmental Forcing, Ann Rev Mar Sci, 1, 213–244, https://doi.org/10.1146/annurev.marine.010908.163742, 2009.

Weiss: CO2 solubility, 1974.

Weiss, R. and Price, B.: Nitrous oxide solubility in water and seawater, Mar Chem, 8, 347–359, 1980.

Wiberg, P. L., Carr, J. A., Safak, I., and Anutaliya, A.: Quantifying the distribution and influence of non-uniform bed properties in shallow coastal bays, Limnol Oceanogr Methods, 13, 746–762, https://doi.org/10.1002/lom3.10063, 2015.

Wickham H, Averick M, Bryan J, Chang W, McGowan LD, François R, Grolemund G, Hayes A, Henry L, Hester J, Kuhn M, Pedersen TL, Miller E, Bache SM, Müller K, Ooms J, Robinson D, Seidel DP, Spinu V, Takahashi K, Vaughan D, Wilke C, Woo K, Yutani H (2019). “Welcome to the tidyverse.” _Journal of Open Source Software_, *4*(43), 1686. doi:10.21105/joss.01686 <https://doi.org/10.21105/joss.01686>.

https://doi.org/10.5194/egusphere-2026-4232
Preprint. Discussion started: 4 August 2026
© Author(s) 2026. CC BY 4.0 License.

Yang, M., Bell, T. G., Brown, I. J., Fishwick, J. R., Kitidis, V., Nightingale, P. D., Rees, A. P., and Smyth, T. J.: Insights from year-long measurements of air-water CH4 and CO2 exchange in a coastal environment, Biogeosciences, 16, 961–978, https://doi.org/10.5194/bg-16-961-2019, 2019.

Zhu, Q. and Wiberg, P. L.: The Importance of Storm Surge for Sediment Delivery to Microtidal Marshes, J Geophys Res Earth Surf, 127, https://doi.org/10.1029/2022JF006612, 2022.

Zhu, Q. and Wiberg, P. L.: Effects of Seasonal Variations in Seagrass Density and Storms on Sediment Retention and Connectivity Between Subtidal Flats and Intertidal Marsh, J Geophys Res Biogeosci, 129, https://doi.org/10.1029/2023JG007785, 2024.

Zhu, Q., Wiberg, P. L., and Reidenbach, M. A.: Quantifying Seasonal Seagrass Effects on Flow and Sediment Dynamics in a Back-Barrier Bay, J Geophys Res Oceans, 126, https://doi.org/10.1029/2020JC016547, 2021.